The September 24, 2013, Mw7.7 Makran Earthquake

Francois Ayoub, Shengji Wei, Linsen Meng, Jean-Philippe Avouac, Jean-Paul Ampuero, Sebastien Leprince, Romain Jolivet, Don Helmberger

We characterize the source of the Mw 7.7 earthquake which occurred in southwestern Pakistan on 09/24/13 combining remote-sensing and seismological observations. Measurement of surface displacement from cross-correlation of optical images (Landsat 8 provided by the USGS) reveal a 200km long surface ruptrure. Fault slip is essentially strike-slip and reached up to 10m. The dissymmetry of surface displacement indicates a north dipping fault consistent with the 45° dipangle of the north dipping fault in the W phase CMT. Back-propagation of teleseismic waves reveals an unilateral rupture propagating to the SW at about 3.5km/s (possibly supershear). Finite-source modeling of teleseismic waveforms shows that the rupture initiated on a sub-vertical subfault and then propagated to the southwest on a 45°dipping faults segment, the total duration is about 60s and the average rupture velocity is estimated to 3km/s. The rake shows nearly purely strike-slip motion. Rise-times are estimated to less than 8s in general indicating a clear pulse-like rupture.The earthquake was able to propagate along a misoriented pre-existing fault, most probably a thrust fault within the Makran accretionary prisme. the thrust fault was reactivated with strike-slip motion despite the NS horizontal compression in the region. Paradoxically, the earthquake was unable to propagate along the more optimally oriented fault segment north of the rupture, where most of the aftershocks were observed. This earthquake demonstrates that large ruptures can develop on severely misoriented faults and that dynamic stresses can induce large slip with a rake inconsistent with the pre-earthquake stress field. These characteristics require strong dynamic weakening.

Ground displacement measured from Optical Image Correlation

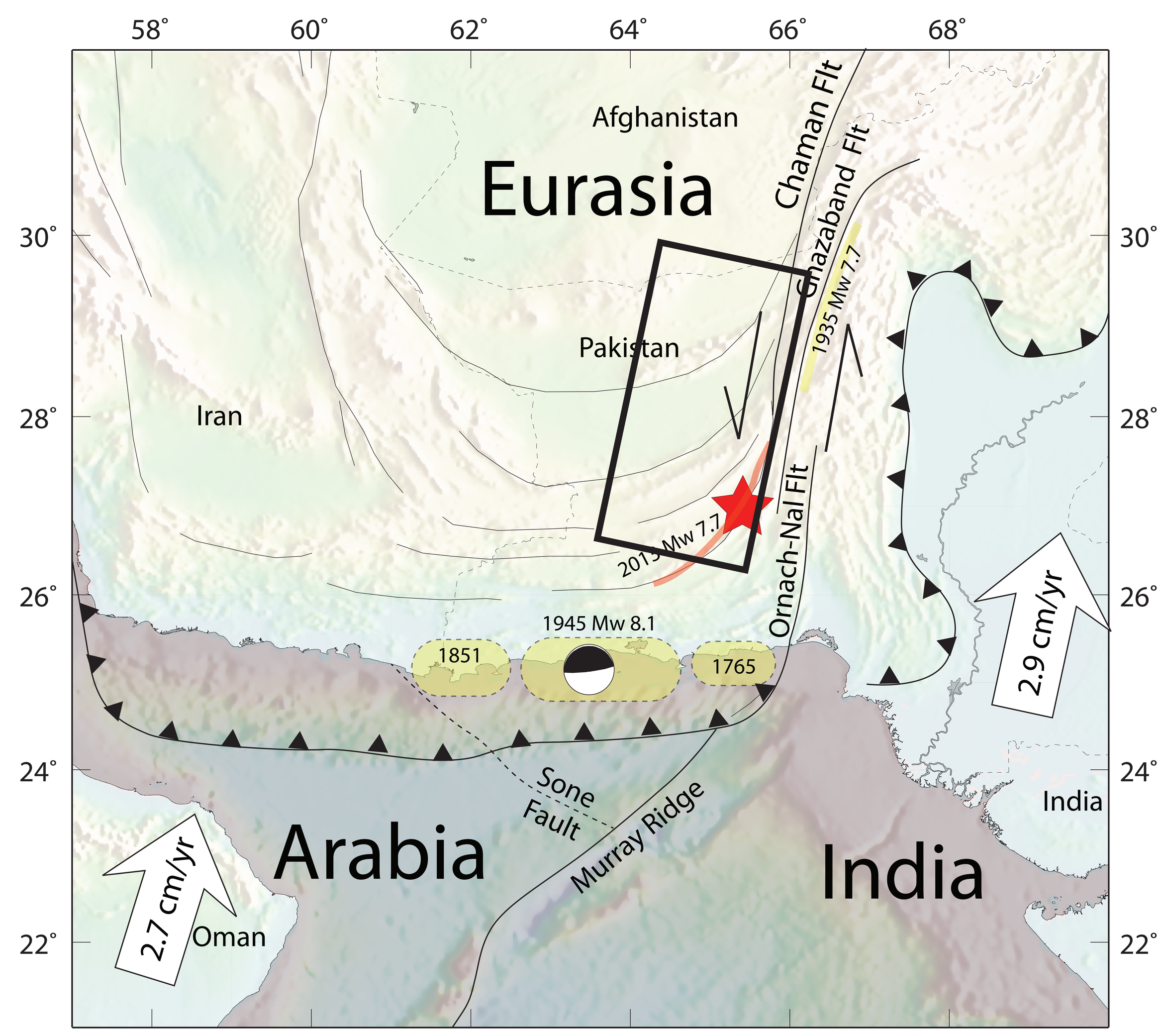

Figure 1: Tectonic Setting (modified form Byrne et al (1992). The earthquake occurred at the southern tip of the Chaman fault, the major left-lateral fault accomodating the northward motion of India relative to Eurasia. Box show location of the Landsat-8 images used in this study.

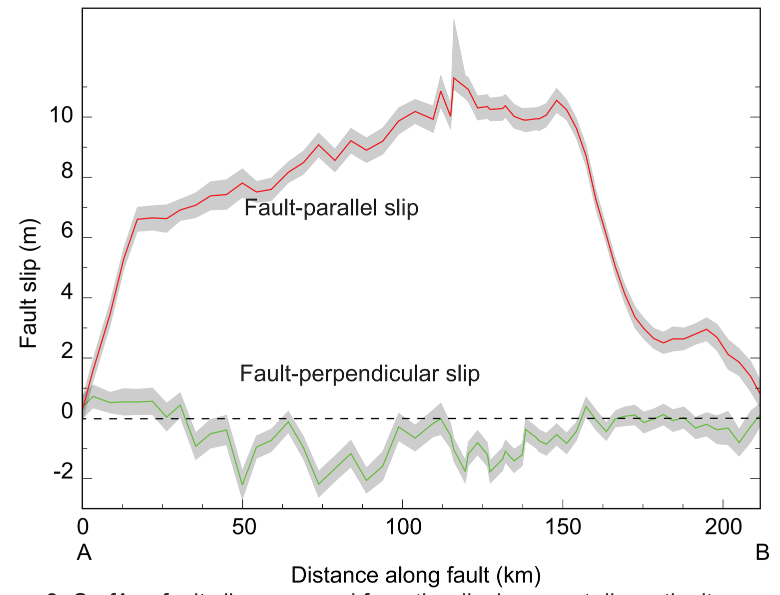

Figure 3: SurfAce fault sllp measured from the displacement discontinuity across the fault trace.

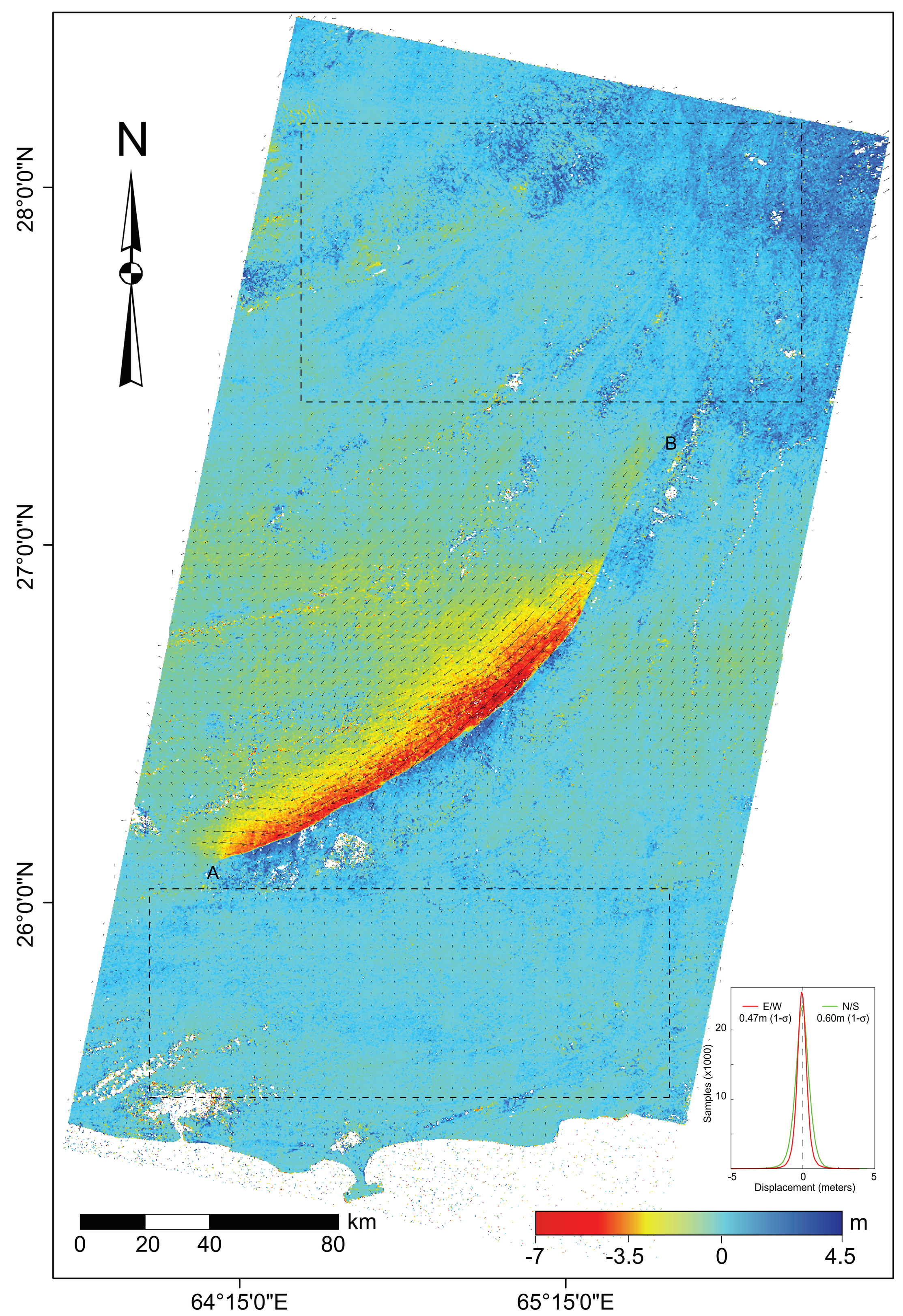

Figure 2: Surface displacement measured from cross-correlation of two pairs of Landsat-8 images (15m GSD) using COSI-Corr (Leprince et al, 2007). Color shading shows EW component of the dipslacement field (240m GSD, 64x64 correlation window). Inset shows histogram of EW and NS displacements within the two areas with presumably null displacement outlined with dashed line. The two pairs (North and South) of displacement maps have been mosaiced.
South part:
pre EQ: LC81540422013253LGN00 acquired 09/10/13
post EQ: LC81540422013269LGN00 acquired 09/26/13
North part:
pre EQ: LC81540412013253LGN00 acquired 09/10/13
post EQ: LC81540412013269LGN00 acquired 09/26/13

Back-projection of Japan P data 0.5-2Hz

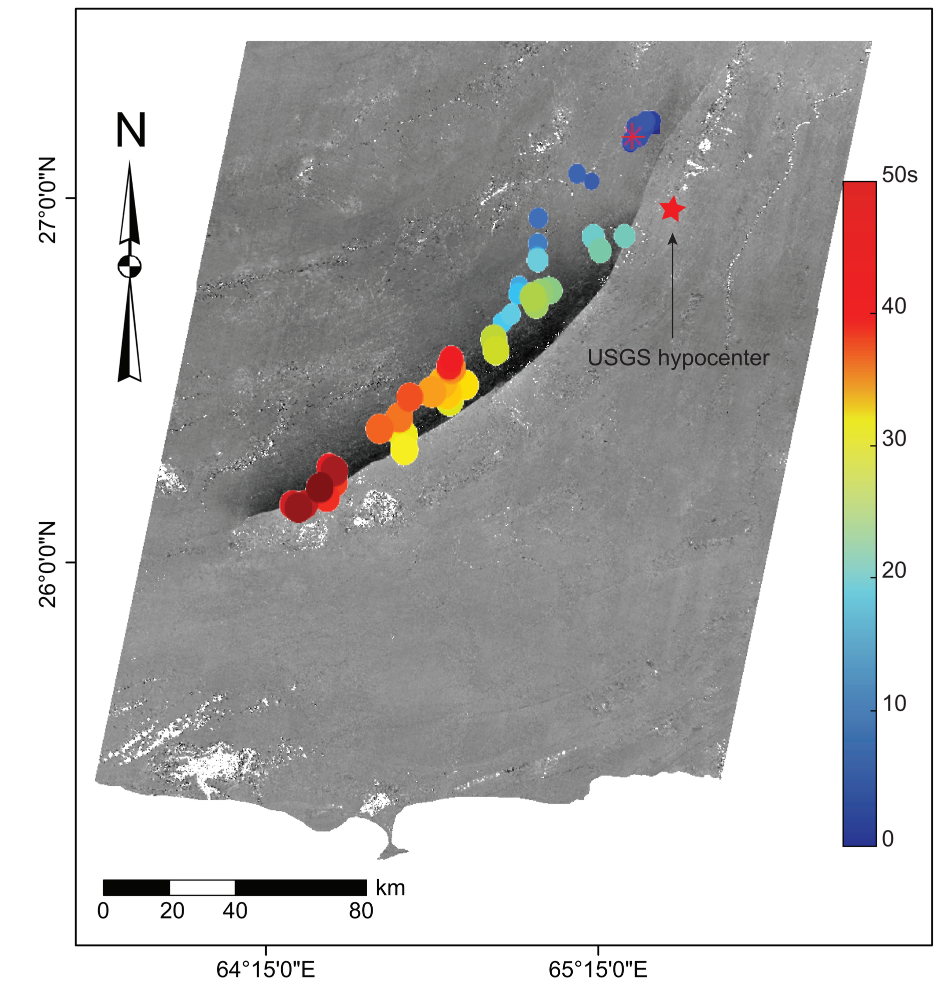

Figure 4: Rupture process imaged from back-projection of teleseismic P waves recorded by the Japanese seismic network using the MUSIC array processing technique [Meng et al., 2011]. Frequency band: 0.5-2Hz. Dots show locations of sources with color indicating time of each window center. First window centered on first P arrival. Sliding window duration: 10s.

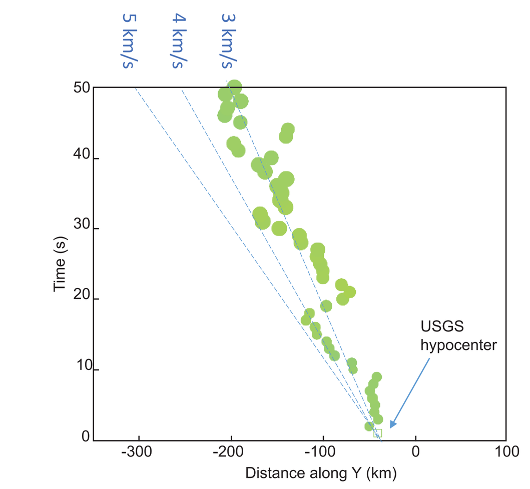

Figure 5: The back-projection results indicate unilateral rupture with average speed of~ 3.5 km/s

REFERENCES

Byrne, D. E., L. R. Sykes, and D. M. Davis (1992), Great thrust earthquakes and aseismic slip along the plate boundary of the Makran subduction zone, Journal of Geophysical Research-Solid Earth, 97(B1), 449-478.Ji, C., D. Wald, and D. V. Helmberger (2002), Source Description of the 1999 Hector Mine, California Earthquake, Part I: Wavelet Domain Inversion Theory and Resolution Analysis, Bull. Seismol. Soc. Am., 92(4), 1192-1207.

Leprince, S., S. Barbot, F. Ayoub, and J. P. Avouac (2007), Automatic and precise orthorectification, coregistration, and subpixel correlation of satellite images, application to ground deformation measurements, Ieee Transactions on Geoscience and Remote Sensing, 45(6), 1529-1558.

Meng, L. S., A. Inbal, and J. P. Ampuero (2011), A window into the complexity of the dynamic rupture of the 2011 Mw 9 Tohoku-Oki earthquake, Geophysical Research Letters, 38.

Finite Source Model

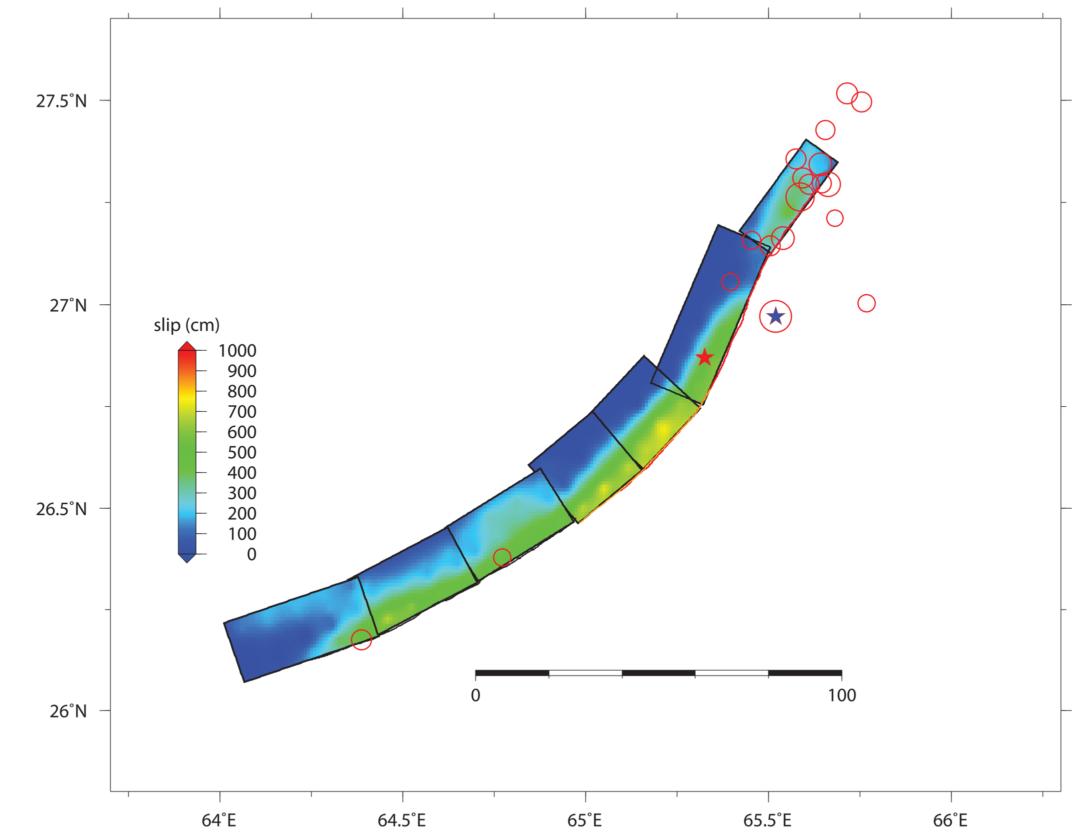

Figure 6: Slip distribution in map view determined from the joint inversion of surface displacements and teleseismic waveforms using the technique of Ji et al (2002)

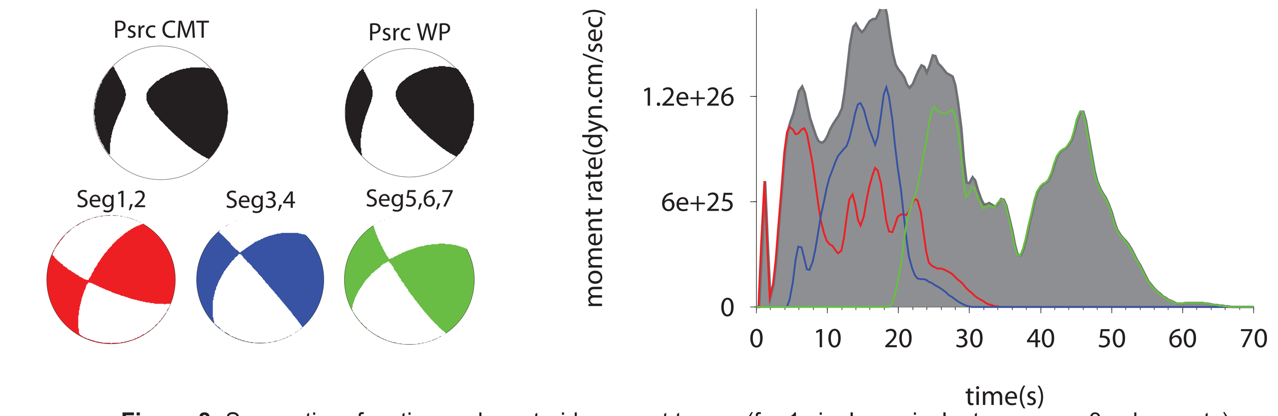

Figure 8: Source time-function and centroid moment tensor (for 1 single equivalent source or 3 sub-events) cooresponding to our best fitting finite source model. Also shown is the CMT derived from point source modeling of the W phase.

Figure 7: Slip distribution and isochrons (in seconds) of rupture front propagation

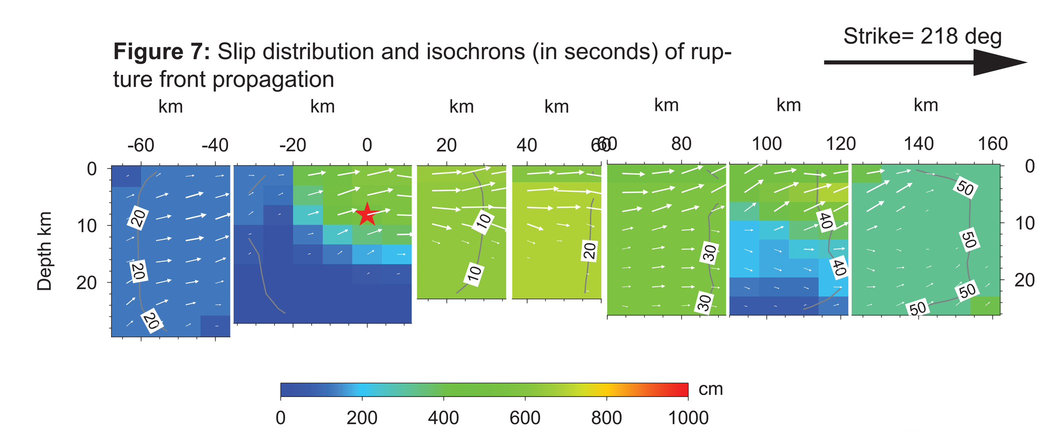

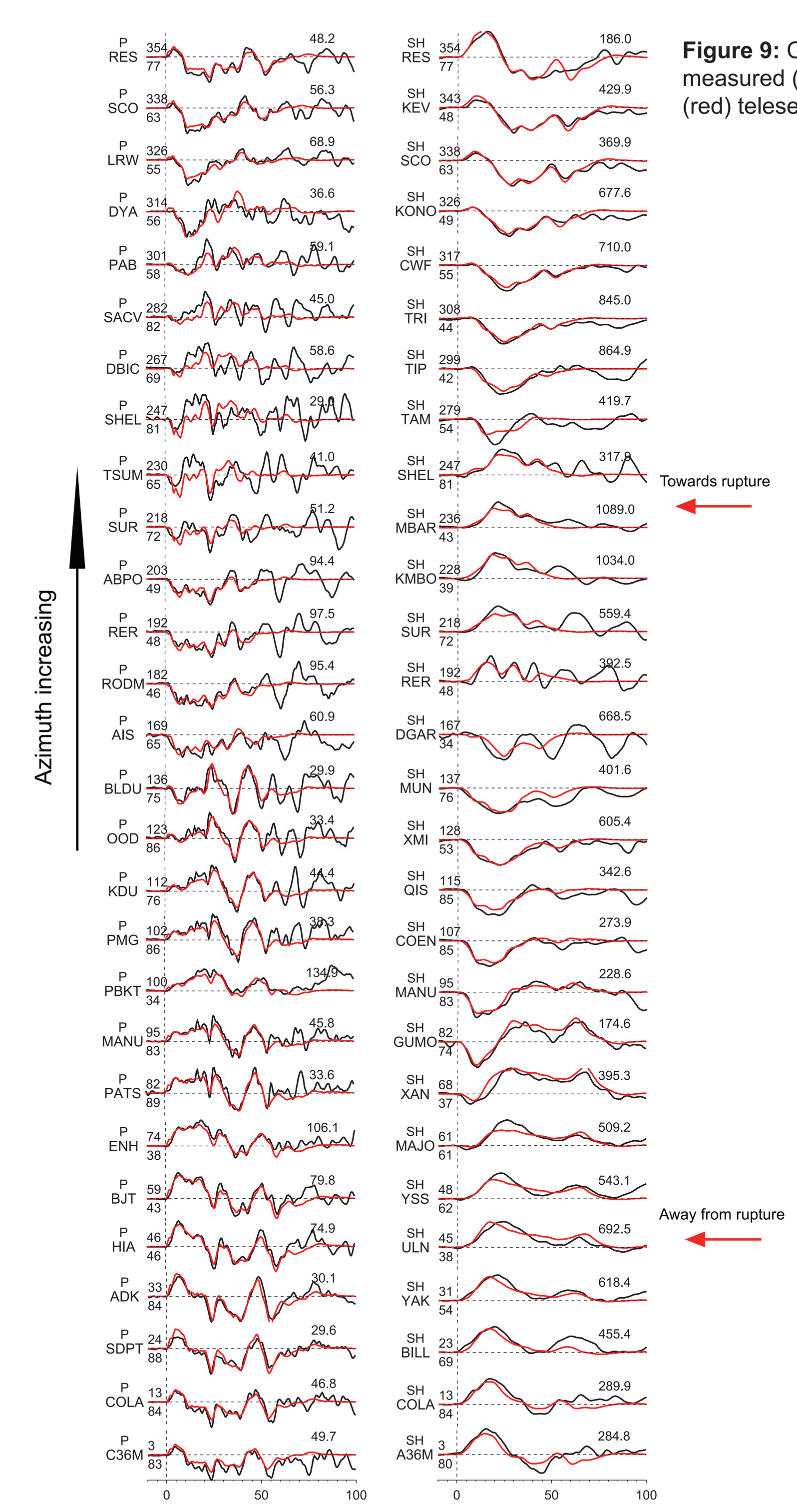

Figure 9: Comparison between measured (black) and synthetic (red) teleseismic waveforms

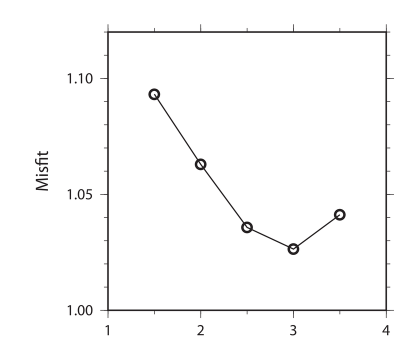

Figure 10: Sensitivity of misfit to assumed rupture velocity.

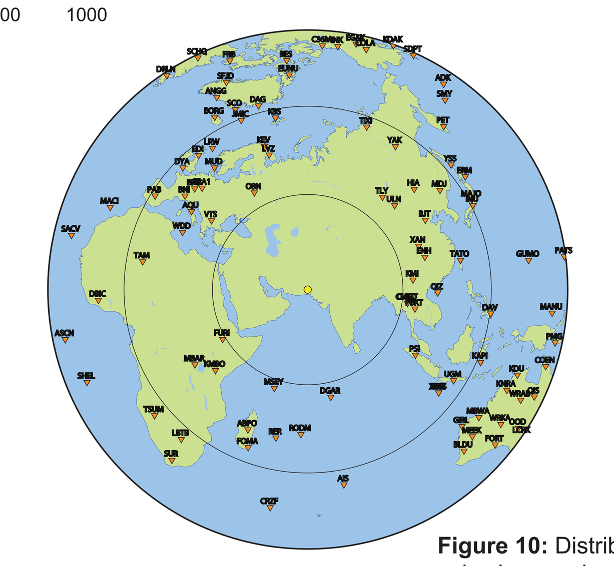

Figure 10: Distribution of teleseismic records used in this study